

1-2012

Approximation of Range in Materials as a Function of Incident Electron Energy

Gregory Wilson
Utah State University

JR Dennison
Utah State University

Follow this and additional works at: https://digitalcommons.usu.edu/graduate_pubs

 Part of the [Physics Commons](#)

Recommended Citation

Gregory Wilson and JR Dennison, "Approximation of Range in Materials as a Function of Incident Electron Energy," *IEEE Trans. on Plasma Sci.*, 40(2), 305-310 (2012). DOI: 10.1109/TPS.2011.2176515

This Article is brought to you for free and open access by the Browse all Graduate Research at DigitalCommons@USU. It has been accepted for inclusion in Graduate Student Publications by an authorized administrator of DigitalCommons@USU. For more information, please contact digitalcommons@usu.edu.

Approximation of Range in Materials as a Function of Incident Electron Energy

Gregory Wilson and JR Dennison

Abstract—A simple composite analytic expression has been developed to approximate the electron range in materials. The expression is applicable over more than six orders of magnitude in energy (<10 eV to >10 MeV) and range (10^{-9} m to 10^{-2} m), with uncertainty of $\leq 20\%$ for most conducting, semiconducting and insulating materials. This is accomplished by fitting data from two standard NIST databases [ESTAR for the higher energy range and the electron IMFP (Inelastic Mean Free Path) for the lower energies]. In turn, these data have been fit with well-established semi-empirical models for range and IMFP that are related to standard materials properties (e.g., density, atomic number, atomic weight, stoichiometry, band gap energy). Simple relations between the IMFP and the range, based on the continuous-slow-down approximation, are used to merge results from the two databases into a composite range expression. A single free parameter, termed the effective number of valence electrons per atom N_V , is used to predict the range over the entire energy span.

Index Terms—range, inelastic mean free path, electron scattering, spacecraft charging

NOMENCLATURE

b	Stopping power proportionality constant.
c	Speed of light <i>in vacuo</i> .
CSDA	Continuous Slow Down Approximation.
\dot{D}	Dose rate.
\bar{E}	Mean energy lost per collision.
E_b	Electron beam energy.
E_{gap}	Band gap energy.
E_{HI}, E_{LO}	Energies to determine n from the Bethe-Joy formula range extremes for NIST databases.
E_{min}	Energy at the minimum in the mean free path curve.
E_{max}	Energy at maximum secondary electron yield, δ_{max} .
E_p^{eff}	Effective plasmon energy.
\hbar	Reduced Planck's constant.
J_b	Electron beam current density.
k	Empirical constant in the Bethe Joy formula.
k_{RIC}	RIC proportionality constant.

M_A	Atomic weight.
m_e	Electron rest mass.
n	Stopping power exponent.
N_A	Avogadro's number.
N_V^{eff}	Effective number of valence electrons.
q_e	Electron charge.
R	Electron range (penetration depth).
RIC	Radiation induced conductivity.
S_{CSDA}	Electron stopping power in CSDA.
v	Electron velocity.
Z_A	Atomic number.
β, γ, C, D, U	Coefficients used in the TPP-2M formula.
δ_{max}	Maximum secondary electron yield.
Δ_{SE}	Secondary electron yield.
Δ	RIC power exponent.
ϵ_0	Permittivity of free space.
$\bar{\lambda}$	Inelastic mean free path at \bar{E} .
λ_{SE}	Secondary electron inelastic mean free path.
λ_{IMFP}	Inelastic mean free path.
λ_{min}	Inelastic mean free path at E_{min} .
ρ_m	Mass density.
σ_{RIC}	Radiation induced conductivity.

I. INTRODUCTION

The range, R , or maximum distance an electron of a given incident energy can penetrate through a material before all kinetic energy is lost and the electron comes to rest, is a common way to parameterize electron interactions with materials. The range is used in spacecraft charging calculations to predict the charge distribution of deposited electrons in materials and to model secondary and backscattered electron emission. It is also used to predict the distribution of energy deposited by incident electrons as they traverse a material; this distribution is further used to model radiation induced conductivity. It is therefore important for spacecraft charging models to have a realistic, reasonably accurate, and efficient expression to predict the approximate range of electron energies commonly encountered in space plasma fluxes, from ~ 10 eV to ~ 10 MeV. The expression needs to be readily implemented for a wide array of conducting, semiconducting and insulating spacecraft materials with a minimal number of fitting parameters.

The Lichtenberg tree in Fig. 1 offers dramatic visual evidence of the validity of the range of electrons in a material. The white line seen at the center of the side view results from melting of the PMMA plastic target during discharge, as electrons deposited in a narrow distribution at a depth of $R \approx 3$

Research was supported by funding from the NASA James Webb Space Telescope Program through Goddard Space Flight Center and a Utah State University Undergraduate Research and Creative Opportunities grant.

Greg Wilson and JR Dennison are with the Materials Physics Group in the Physics Department at Utah State University in Logan, UT 84322 USA (e-mail: GregdWilson@gmail.com, JR.Dennison@usu.edu).

Color versions of one or more figures in this paper are available online at <http://ieeexplore.ieee.org>.

Digital object identifier .

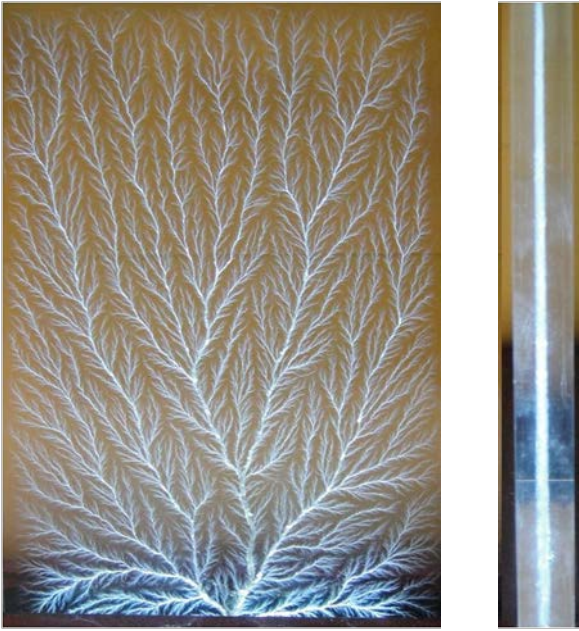


Fig. 1. Front (Left) and side (Right) views of a Lichtenberg discharge tree. The white line (Right) indicates the narrow distribution of deposited charge from a ~ 1 MeV electron beam at $R \approx 3$ mm in a PMMA sample.

mm by a monoenergetic ~ 1 MeV electron beam are released.

II. THEORY

The desired range expression can be developed by merging well known semi-empirical models for the interaction of electrons with materials in different energy regimes by employing the continuous-slowing-down approximation (CSDA). In the CSDA, the rate of energy loss, dE/dz (or total stopping power, S_{CSDA}), at every position along the penetration path is assumed constant; variations in energy-loss rate with energy, E , or penetration depth, z , are neglected. For a given incident energy, E_b , the CSDA range is obtained by integrating total stopping power over the full penetration depth such that $E_b = \int_0^{R(E_b)} (dE/dz) dz$ [1, 2].

In the CSDA with a constant energy-loss rate,

$$\frac{dE}{dz} \equiv S_{CSDA}(E_b) = E_b/R = \bar{E}/\bar{\lambda} = E_{min}/\lambda_{min} \quad (1)$$

Here \bar{E} is equal to mean energy lost per collision occurring at mean free path $\bar{\lambda} \equiv \lambda_{IMFP}(\bar{E})$, and E_{min} is the energy at the minimum in the inelastic mean free path curve at $\lambda_{min} \equiv \lambda_{IMFP}(E_{min})$. A reasonable approximation for \bar{E} is the geometric mean of the effective plasmon energy and the bandgap energy, E_{gap} , times an empirically determined factor of 2.8 [3]:

$$\bar{E} = 2.8 \left[(E_p^{eff})^2 + (E_{gap})^2 \right]^{1/2} \quad (2)$$

The effective plasmon energy, E_p^{eff} , for an arbitrary atomic or molecular material is defined in analogy with the bulk free-electron plasma energy for conductors—which is proportional to the square root of the number of valance electrons per atom or molecule—as

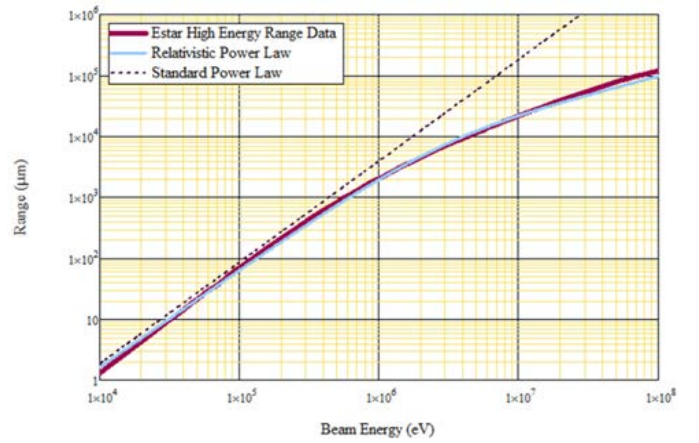


Fig. 2. Comparison between the standard power law and the relativistic power law for Al. The relativistic power law allows approximations for energies up to 10 MeV with percent errors $\sim 20\%$.

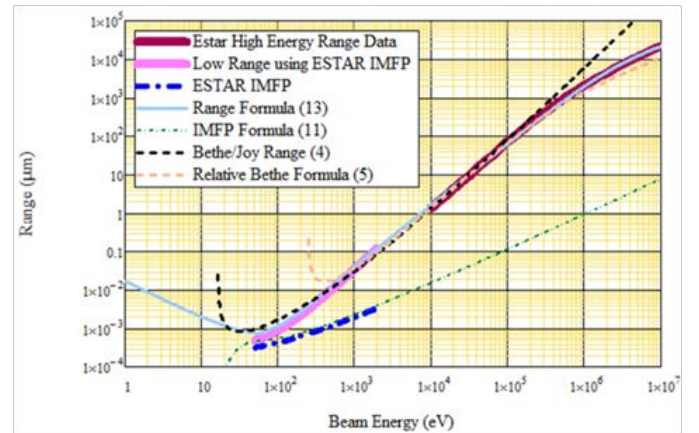


Fig. 3. Comparison between several range approximations and the data from the ESTAR database for Al [4]. The IMFP data for Al are also plotted, along with the TPP-2M IMFP formula for $\lambda_{IMFP}(E)$ [5].

$$E_p^{eff} = \hbar (N_V^{eff} N_A \rho_m q_e^2 / m_e \varepsilon_0 M_A)^{1/2} \quad (3)$$

Following the analogy, the free parameter N_V^{eff} is termed the effective number of valance electrons per atom, as discussed further below. Here q_e and m_e are the electron charge and rest mass, \hbar is the reduced Planck's constant, ε_0 is the permittivity of free space, N_A is Avogadro's number, M_A is the atomic weight, and ρ_m is the mass density [4].

Tabulated values of the electron ranges at high energies using the CSDA can be found in the NIST ESTAR database spanning incident energies from $E_{HI} \sim 20$ keV to ~ 1 GeV [5].

The CSDA can also be applied to lower energy ranges. The NIST electron inelastic mean free path (IMFP) database [6] has tabulated values and semi-empirical fits for the IMFP—which is closely related to the range as shown below—which are valid for energies from ~ 30 eV to $E_{LO} \sim 1$ keV.

Thus, in order to create an analytic expression for the full span of desired energies, the problem can be broken into three parts according to energy of the incident electron: a high energy range for $E_b > E_{LO} \equiv 1$ keV; a mid-energy range for $\bar{E} < E_b < E_{LO}$; and a low energy range for energies $E_b < \bar{E}$.

A. High Energy Range

Range values at high energy are tabulated in the NIST ESTAR database [5]. The non-relativistic Bethe-Joy range

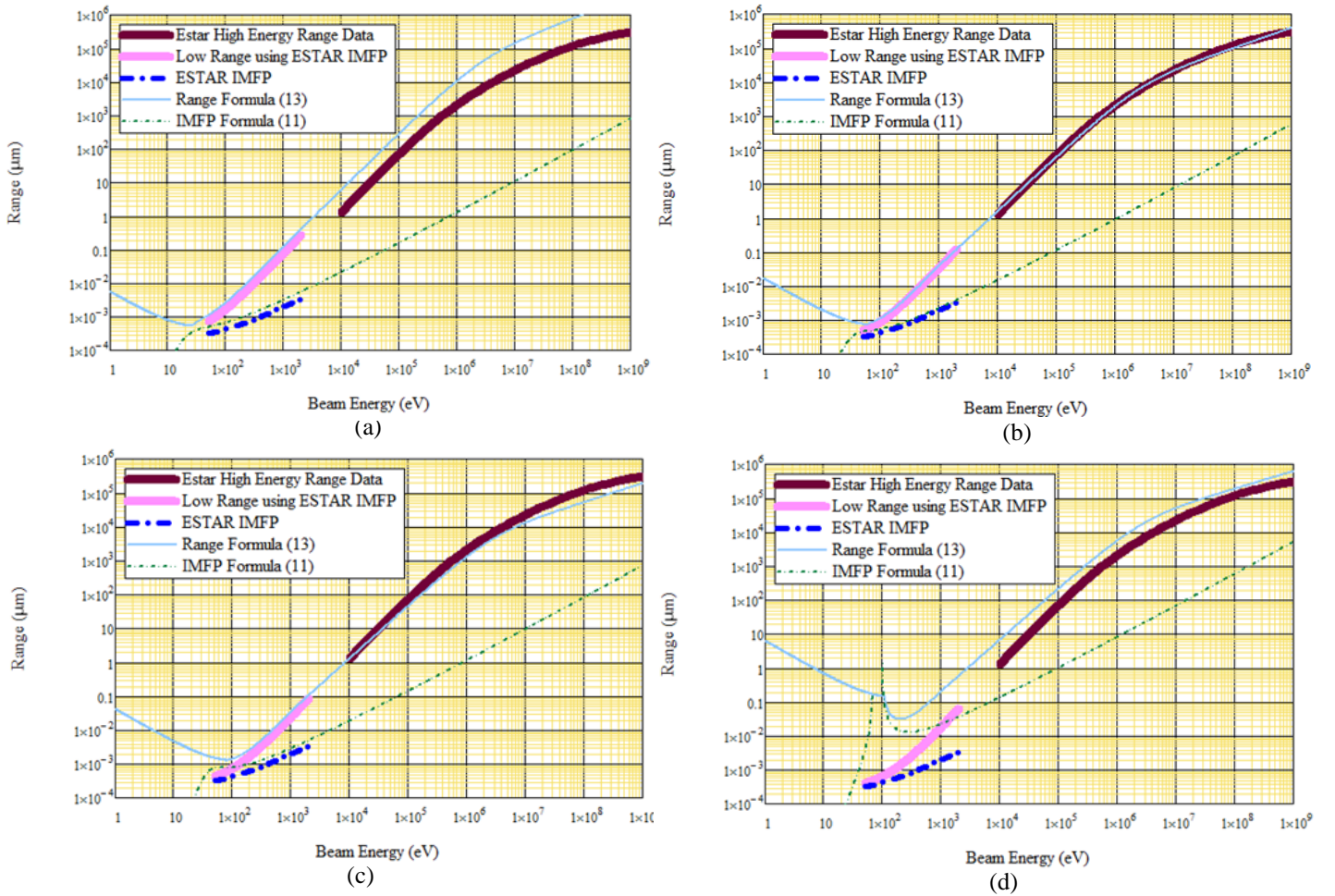


Fig. 4. Graphs showing the variation of the range expression for Al, as a function of the single fitting parameter N_V^{eff} . For graphs (a) through (d), $N_V^{eff} = 1, 5$ (best fit), 10 and 18, respectively.

expression based on the Bethe stopping power formula [7] has been extended to lower energies by Joy and Luo [8] and Tanuma [9], with the addition of a fixed empirical constant, $k=0.8$ and by replacing the mean excitation energy, J , in the Bethe expression with a closely related empirical parameter, J_{exp} . The resulting Bethe-Joy-Luo expression

$$R_{BJL}(E_b) = \left[\frac{(4\pi\epsilon_0)^2 M_A}{2\pi q_e^4 Z_A \rho m} \right] E_b^2 \left[\ln \left(\sqrt{\frac{E}{N_V^{eff} E}} \left[\frac{E_b}{N_V^{eff} E} + k \right] \right) \right]^{-1} \quad (4)$$

is used to fit the data up to $\sim 10^5$ eV, above which a relativistic correction becomes significant [10]. Z_A is the atomic number and we have replaced the Joy-Luo empirical parameter J_{exp} with our empirical parameter $N_V^{eff} E$. A relativistic extension of this equation is

$$R_{BJL}^{rel}(E_b) = \frac{\left[\frac{(4\pi\epsilon_0)^2 M_A}{2\pi q_e^4 Z_A \rho m} \right] E_b \frac{m_e c^2}{2} \left[1 - \left(1 + \frac{E_b}{m_e c^2} \right)^{-2} \right]}{\left\{ \ln \left[\frac{\left[\frac{E}{\sqrt{2} m_e c^2} \left[1 - \left(1 + \frac{E_b}{m_e c^2} \right)^{-2} \right] \right]}{E \left(1 + \frac{E_b}{m_e c^2} \right)^{-2}} + k \right] \right\} \left[1 - \left(1 + \frac{E_b}{m_e c^2} \right)^{-2} \right]} \quad (5)$$

A common approximation for $R(E_b)$ for ~ 1 keV $< E_b < 50$ keV is a simple power law formula, with a stopping power exponent n ;

$$R_{HE}(E_b) = \frac{N_V^{eff} \left(\frac{1}{2} m_e v^2 \right)}{dE/dx} = b' E_b^{1+n} \quad \text{with } S \equiv dE/dx \propto E_b^{-n} \quad (6)$$

where in the non-relativistic limit, the incident free electron energy is $E_b = q_e V = N_V^{eff} \left(\frac{1}{2} m_e v^2 \right)$. In general, physical constraints require $0 \leq n \leq 1$ [1]. Numerous power law models have been developed for different classes of materials, with $0.35 \leq n \leq 0.67$ [1 and references therein]. Indeed, Eq. (4)—in the limit where the $\ln(E_b)$ term is negligible—reduces to a limiting-case Thomson-Whiddington $n=1$ power law dependence [11].

A simple power law approximation applicable to higher incident energies is found by inserting the relativistic velocity equation $v^2 = c^2 \left[1 - \left(1 + \frac{E}{m_e c^2} \right)^{-2} \right]$ into Eq. (6):

$$R_{HE}^{rel}(E_b) = b E_b^n \left[1 - \left[1 + \left(\frac{E_b}{N_V^{eff} m_e c^2} \right) \right]^{-2} \right] \quad (7)$$

Above ~ 10 MeV (higher energies for lower Z_A materials), total bremsstrahlung radiation energy losses—proportional to E^2 using the Kramers efficiency relation—dominate energy losses due to collisions. Figure 2 shows the fit to tabulated

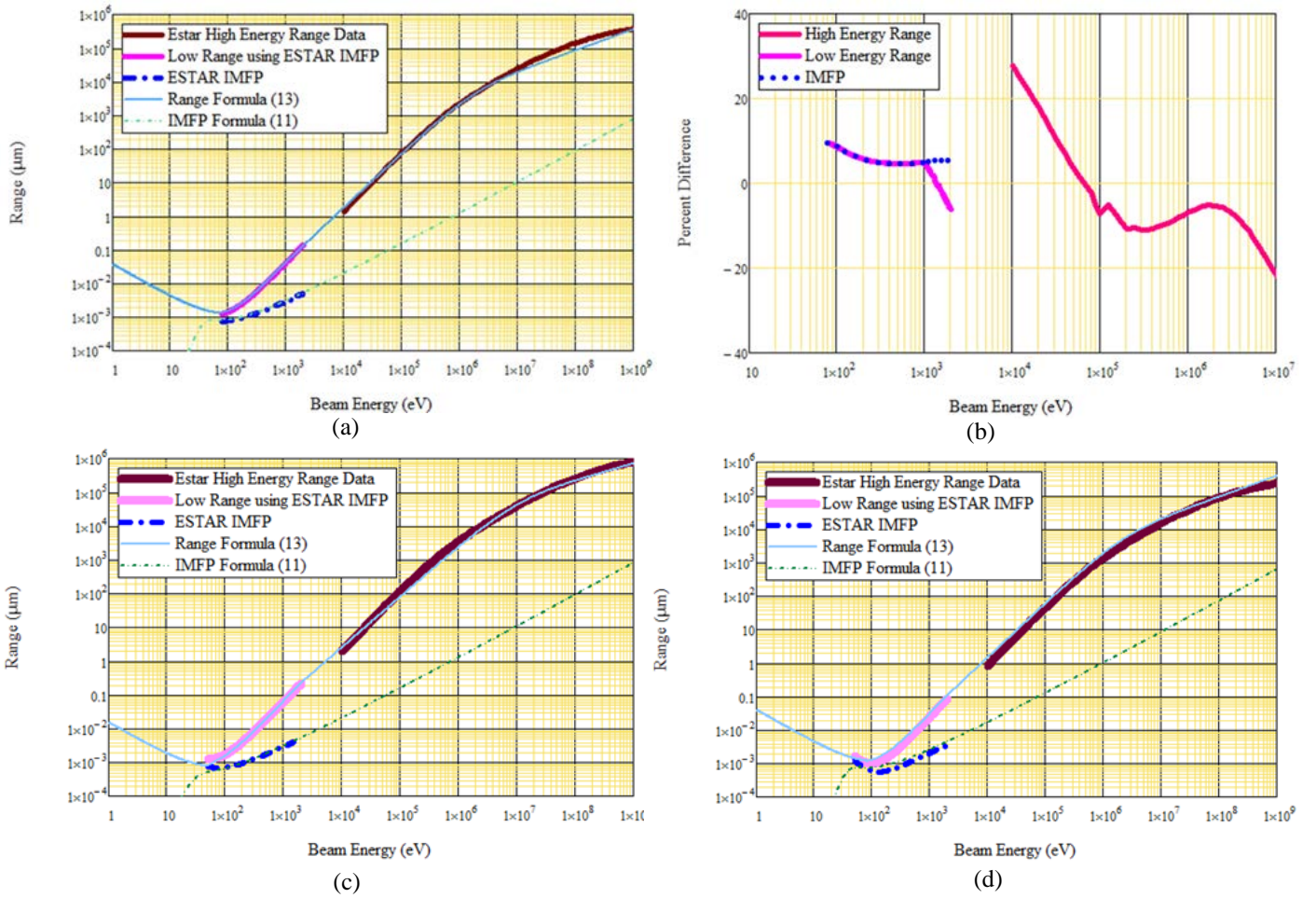


Fig. 5. (a) Comparison of the range formula for SiO₂ with $N_V^{eff} = 6.0$. (b) Residual plot of SiO₂ range data in Fig 5. (c) Comparison of the range formula for Kapton with $N_V^{eff} = 2$. (d) Comparison of the range formula for Al₂O₃ with $N_V^{eff} = 5.0$.

data for Al from the ESTAR database, using both non-relativistic and relativistic power law expressions, Eqs. (6) and (7), respectively. Figure 3 shows fits to the Al data using several range approximation formulas.

The stopping power exponent n and proportionality constant b can be expressed in terms of N_V^{eff} by matching the slope and magnitude of the approximate power law formula, Eq. (6) or (7), to the Bethe-Joy-Luo and mid-energy range expressions, respectively. n is determined by requiring that the slope of the range power law from Eq. (6) for $R_{HE}(E)$ matches the Bethe-Joy-Luo formula—Eq. (4)—at two non-relativistic energies, E_{LO} and E_{HI} , in the regime where both expressions give reasonable results. $E_{HI} \equiv 20$ keV is the lower energy at which data are available for all materials in the ESTAR database and $E_{LO} \equiv 1$ keV is the upper energy at which data are available for all materials in the IMFP database. This leads to an expression for the stopping power exponent

$$n(N_V^{eff}; \rho_m, M_A, E_{gap}) = \left\{ \ln \left[\frac{\ln \left[\sqrt{e/2} \left(\frac{E_{HI}}{N_V} + k \right) \right]}{\ln \left[\sqrt{e/2} \left(\frac{E_{LO}}{N_V} + k \right) \right]} \right] \left[\ln \left[\frac{E_{LO}}{E_{HI}} \right] \right]^{-1} + 1 \right\} \quad (8)$$

The magnitude of the high energy range expression, Eq. (7), is normalized to the mid-energy expression—Eqs. (10) and (11) developed in Section B—at E_{LO} , by setting

$$b(N_V^{eff}; \rho_m, M_A, E_{gap}) = \frac{E_{LO}^{1-n} \lambda_{IMFP}(E_{LO}) (1 - e^{-E_{LO}/\bar{E}})^{-1}}{\bar{E} \left(\left[1 - \left[1 + \left(\frac{E_{LO}/N_V}{m_e c^2} \right)^2 \right]^{-1} \right) \right)} \quad (9)$$

Note that the only free parameter in Eqs. (8) and (9) is N_V^{eff} , along with \bar{E} which is expressed in terms of N_V^{eff} and the band gap energy, E_{gap} in Eq. (1).

B. Mid-Energy Range

Direct extrapolation of the range from the ESTAR data to lower energies is not valid for energies comparable to the atomic electronic structure, typically a few keV and below, because the discrete energy nature of the collisions becomes important. However, a simple extension of the CSDA to lower energies can relate the range to the electron IMFP, where

$$\frac{dE}{dz} = E_b / R(E_b) = \left[\bar{E} / \lambda_{IMFP}(E_b) \right] (1 - e^{-E_b/\bar{E}}) \quad (10)$$

Here the stopping power is again assumed equal to the total energy lost (incident energy, E_b) divided by the total distance traveled (range, $R(E_b)$). This is set equal to the mean energy lost per collision, \bar{E} , divided by the mean distance traveled per collision all times the probability that a collision occurs,

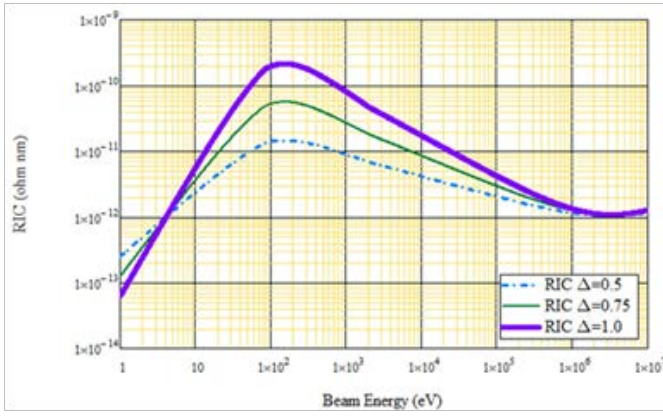


Fig. 7. RIC as a function of energy in the CSDA for polyimide.

$(1 - e^{-R/\bar{\lambda}}) = (1 - e^{-E_b/\bar{E}})$. For $\bar{E} > E_b > E_{HI}$, $\lambda_{IMFP}(E_b)$ is assumed to be given by the TPP-2M formula [12] used in conjunction with the NIST IMFP database [6]:

$$\lambda_{IMFP}(E) = E [E_p^{eff}]^{-2} [\beta \ln(\gamma E) - CE^{-1} + DE^{-2}]^{-1} \quad (11)$$

where

$$\beta \equiv [-0.1 + 2.783\bar{E}^{-1} + 0.069\rho_m^{0.1}] (eV\text{\AA})^{-1} \quad (12)$$

$$\gamma \equiv [0.191 \rho_m^{-1/2}] (eV^{-1})$$

$$C \equiv [1.97 - 0.91 U] (\text{\AA}^{-1})$$

$$D \equiv [53.4 - 20.8 U] (eV \text{\AA}^{-1})$$

$$U \equiv [N_V^{eff} \rho_m] / M_A (cm^{-3})$$

Because of the shallow core levels (generally with binding energies < 30 eV) that may contribute significant intensity to the energy-loss function, there arises an ambiguity in the choice of the value of the number of valence electrons [12]. Powell *et al.* used the bulk free-electron plasma energy value for N_V^{eff} in Eq. (12) for elemental conductors, and obtained good agreement with optical absorption and inelastic electron scattering data which are often described in terms of a parameter termed the “effective number of electrons per atom” [9,12,13]. Powell *et al.* also found good agreement for studies of other materials, including, semiconductors, insulators, and organic and inorganic compounds, by determining the parameter N_V^{eff} from sum rule considerations of the scattering contributions from electrons in particular atomic shells or subshells [9,12,13]. There are extensive discussions on the best way to approximate these fitting parameters, based solely on materials properties [8,12,14]. Gries used an alternate approach to model the IMFP, based on empirical fits and an “effective Z parameter”, Z^* , described as the “nominal effective number of interaction-prone electrons per atom” [14]; note, however, that Tunuma, Powell and Penn took exception to the physical interpretation of this fitting parameter [12].

IMFP data from the NIST database [6] (see thick blue dashed curves in Figs. 3, 4 and 5) were fit well over the mid-energy range using the TPP-2M model given by Eqs. (11) and (12) with N_V^{eff} determined by fits to the ESTAR database [5] through Eqs. (8) and (9) (see thin dashed green curves in Figs. 3, 4 and 5). Once again, by using the proposed TPP-2M equations of Tanuma inserted into Eq. (10), the only free

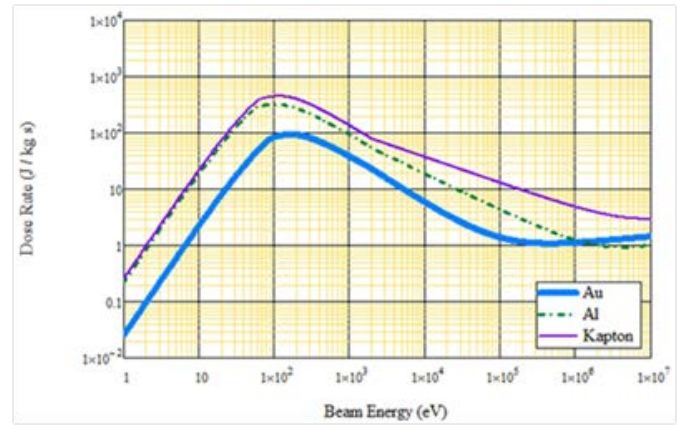


Fig. 6. Dose rate as a function of energy in the CSDA for Au, Al and polyimide.

parameter for the mid-energy range expression is N_V^{eff} , along with the materials constants E_{gap} , M_A , and ρ_m through \bar{E} . While E_{gap} may be considered an additional fitting parameter for semiconductors and insulators, its effect on R is minimal, causing primarily a vertical shift in the range curve within 2% using acceptable band gap energies. Thus, E_{gap} can be treated essentially as an additional tabulated material constant—such as M_A and ρ_m are—derived from independent optical measurements.

C. Low Energy Range

To calculate the range for $E_b < \bar{E}$, we assume in the CSDA that: (i) the energy lost per low energy collision is constant and equal to the mean excitation energy, \bar{E} ; (ii) the IMFP is constant and equal to the IMFP at the mean energy loss or $\lambda_{IMFP}(\bar{E}) = \bar{\lambda}$; and (iii) the probability that an electron undergoes one such inelastic collision falls off as $R/\bar{\lambda} (e^{-R/\bar{\lambda}}) = E_b/\bar{E} (e^{-E_b/\bar{E}})$. This simple low energy approximation avoids the unusual asymptotic behavior exhibited by the TPP-2M expression at energies below \bar{E} that is evident in the thin dashed green curves in Figs. 3, 4, and 5. The resulting expression is consistent with a universal curve of electron IMFP versus kinetic energy [15] observed for a wide range of materials [16], that is consistent with a simple free electron gas model of valence electrons in the material [17].

D. Composite Range Function

The final result is a continuous composite analytic approximation to the range, spanning from < 10 eV to > 10 MeV, with a single fitting parameter, N_V^{eff} :

$$R(E_b; N_V^{eff}) = \begin{cases} \left[\frac{E_b}{\bar{E}} \right] \left[\lambda_{IMFP}(\bar{E}) \frac{(1 - e^{-\bar{E}/\bar{E}})}{(1 - e^{-E_b/\bar{E}})} \right] (1 - e^{-E_b/\bar{E}})^{-1} & ; E_b < \bar{E} \\ \left[\frac{E_b}{\bar{E}} \right] \lambda_{IMFP}(E_b) (1 - e^{-E_b/\bar{E}})^{-1} & ; \bar{E} \leq E_b \leq E_{HI} \\ b E_b^n \left[1 - \left[1 + \left(\frac{E_b}{N_V^{eff} m_e c^2} \right) \right]^{-2} \right] & ; E_b > E_{HI} \end{cases} \quad (13)$$

Figure 4 demonstrates the sensitivity of the composite fit, Equation (10), to N_V^{eff} for a typical conductor, Al. Lower values of N_V^{eff} overestimate the range, while higher values of

Table I. Materials Properties and Fitting Parameters

Material		Fitting Parameter N_V^{eff}	Material Properties				Derived Values				
Name	Formula		ρ_m (gm/cm ³)	Z_A	M_A (amu)	E_{gap} (eV)	n	b ($\mu\text{m}/\text{eV}^{-n}$)	E_p^{eff} (eV)	E_m (eV)	λ_{min} (nm)
Graphite	C	5.3	1.7	6	12.01	0.1	0.642	0.7143	24.87	69.6	0.793
Amorphous C	C	4.0	2.0	6	12.01	0.1	0.676	0.3877	23.43	65.6	0.614
Aluminum	Al	5.0	2.7	13	26.98	0.0	0.668	0.5075	20.31	56.9	0.467
Silicon	Si	5.0	2.33	14	28.09	1.11	0.676	0.5422	18.49	51.9	0.438
Copper	Cu	8.3	8.96	29	63.55	0.0	0.561	0.7821	31.06	87.0	0.422
Germanium	Ge	9.8	5.32	32	72.64	0.66	0.571	1.355	24.32	68.1	0.477
Silver	Ag	10.6	10.5	47	107.87	0.0	0.536	1.217	29.17	81.7	0.416
Gold	Au	12.0	19.32	79	196.97	0.0	0.508	1.261	31.15	87.2	0.371
Polyethylene	[C ₂ H ₄] _n	2.5	0.94	2.65	4.64	2.9	0.727	0.2354	20.43	57.8	0.642
Polyimide	[C ₂₂ H ₁₀ N ₂ O ₅] _n	4.1	1.42	5.01	9.769	2.3	0.678	0.4582	22.17	62.4	0.652
PTFE	[C ₂ F ₄] _n	6.0	2.2	8.01	16.023	6	0.620	0.8794	26.06	78.9	0.865
Aluminum Oxide	Al ₂ O ₃	5.0	3.97	10	30.392	9.9	0.628	0.5188	28.33	84.0	0.746
Silicon Dioxide	SiO ₂	6.0	2.32	9.98	19.99	8.9	0.622	0.895	23.90	71.4	0.818
Glass, Pyrex	doped SiO ₂	6.2	2.32	9.98	19.99	4	0.626	0.8150	24.36	69.1	0.656

N_V^{eff} underestimate the range. Based on the quality of the fits to the database values, the typical uncertainty in N_V^{eff} is estimated to be $\lesssim 10\%$. The residual curve for the fit for Al is shown in Fig. 5(b).

Figures 5(a), 5(c) and 5(d) show best fits to data for three prototypical materials: the conductor Al; the polymeric insulator polyimide (Kapton), and the insulating ceramic Al₂O₃. Table I lists the fitting parameter N_V^{eff} , along with materials properties and derived values, for 14 common spacecraft materials. A more extensive set of fitting parameters for additional materials is currently being developed.

III. APPLICATIONS

The usefulness of an analytical approximation of the range to spacecraft applications can easily be demonstrated by considering expressions for the dose rate and the radiation induced conductivity; both expressions require an energy dependent range expression.

The dose rate, \dot{D} , is defined as the power deposited by incident radiation per unit mass. The dose rate in the CSDA for a homogeneous material is inversely proportional to the volume in which radiation energy is deposited; this volume is approximately equal to the beam cross sectional area times R [18]. Thus,

$$\dot{D} \equiv \partial D / \partial t = \frac{E_b J_b}{\rho_m R q_e} \propto R^{-1} \quad (14)$$

The dose rates for three materials as a function of incident energy are shown in Fig. 6.

Radiation Induced Conductivity (RIC) is the enhanced conductivity that results from the energy deposited in this volume. In the CSDA

$$\sigma_{RIC}(\dot{D}) = k_{RIC} \dot{D}^\Delta \phi \propto R^{-\Delta} \quad (15)$$

with $1/2 < \Delta < 1$ [19]. Figure 7 shows the RIC for Kapton as a function of incident energy for three values of Δ . As expected, RIC effects are generally larger for larger Δ , with the variation largest at the maximum value near $3\bar{E}$ and becoming much

smaller in the relativistic region. The magnitude of RIC exhibits a crossover at ~ 2 eV; however, this is below the energy range for which Equation 10 is valid.

Notice that both \dot{D} and σ_{RIC} exhibit energy dependent maxima as a consequence of the minimum in the range expression. Both curves also have local minima at ~ 3 MeV for Au, as a result of the relativistic correction in Eq. (7) that occurs at lower energies for more dense materials.

Secondary electron (SE) emission is another electron scattering process for which application of the range expression developed here could provide insight. In the CSDA, the SE yield can be expressed as [1]

$$\delta_{SE}(E, N_V^{eff}, \delta_{max}, E_{max}) = \frac{\delta_{max}}{1 - \exp\left[-\frac{R(E)}{\lambda_{SE}}\right]} \left\{ 1 - \exp\left[-\frac{R(E)}{\lambda_{SE}} \left(\frac{E}{E_{max}}\right)^\eta\right] \right\} \quad (16)$$

In a similar vein, Yasuda *et al.* have investigated the SE yield in terms of the relation between the IMFP and the valence electron excitation function (which they approximate by the outer shell ionization function) [20]. Earlier, Ashley and Williams found that the electron stopping power for many polymers was a function of the ratio of the number of valence electrons, N_v , in a monomer unit to its molecular weight, M_A [21]. Burke used their relation to express the secondary electron emission coefficient from polymers as a function of N_v / M_A in a semi-empirical model [22]. Work is underway at USU to develop an expression for the SE yield in terms of the composite range expression, Equation (10). The resulting SE expression would have three independent free parameters; N_V and the maximum SE yield δ_{max} at energy E_{max} .

IV. CONCLUSION

Using the CSDA, a continuous, simple, composite, analytic formula—with a single free parameter, termed the effective number of valence electrons, N_V^{eff} —has been developed to approximate the range (10^{-9} m to 10^{-2} m) over an extended energy span (< 10 eV to > 10 MeV). Agreement with available databases of electron interactions are within $< 20\%$ for many

conducting, semiconducting, and insulating materials. Use of this continuous expression over the extended energy range permits development of continuous expressions over extended energy ranges for dose rate, RIC and (potentially) SE yield. By comparing these extended expressions to data, which are often considerably easier to measure than range, the range formula can be further validated and improved. Continued development may also establish the ability to approximate the fitting parameter, N_V^{eff} , using only material and empirical constants. This would allow construction of an empirical database for materials without the necessity of specific range data.

REFERENCES

1. Reimer, L., 1998, "Scanning Electron Microscopy: Physics of Image Formation and Microanalysis," 2nd Ed., Springer-Verlag, Heidelberg.
2. Spencer, L., 1955, "Theory of Electron Penetration," Phys. Rev. 98, 1597.
3. Alig, R., and S. Bloom, 1975, "Electron-Hole-Pair Creation Energies in Semiconductors," Phys. Rev. Lett. 35, 1522.
4. Pines, D., 1963, *Elementary Excitations in Solids*, Addison-Wesley, Reading, MA.
5. National Institute of Standards and Technology, 2010, "ESTAR, Stopping Power and Range Tables for Electrons," (<http://physics.nist.gov/PhysRefData/Star/Text/ESTAR.html>).
6. National Institute of Standards and Technology, 2010, "NIST Electron Inelastic-Mean-Free-Path Database: Version 1.1," (<http://www.nist.gov/data/nist71.htm>).
7. Bethe, H., and W. Heitler, 1934, "On the Stopping of Fast Particles and on the Creation of Positive Electrons," in Proc. Royal Soc. London. Series A, Containing Papers of a Mathematical and Physical Character 146, 83.
8. Joy D.C., and Luo S., 1989, "An empirical stopping power expression for low energy electrons," Scanning 11, 176.
9. Tanuma, S., C. Powell, and D. Penn, 2005, "Calculations of Stopping Powers of 100 eV to 30 keV Electrons in 10 Elemental Solids," Surf. Inter. Anal. 37, 978.
10. Evans, R.D., 1955, *The Atomic Nucleus*, Internat. Ser. In Pure and Appl. Phys., McGraw-Hill, New York.
11. Whiddington, R., 1914, "The Transmission of Cathode Rays Through Matter," in Proc. Royal Soc. London. Series A, Containing Papers of a Mathematical and Physical Character 89, 554.
12. Tanuma, S., C.J. Powell and D.R. Penn, 1997, "Calculations of Electron Inelastic Mean Free Paths (IMFPs) VI. Analysis of the Gries Inelastic Scattering Model and Predictive IMFP Equation," Surf. Inter. Anal. 25, 25.
13. Powell, C.J., and A. Jablonski, 2000, "Evaluation of Electron Inelastic Mean Free Paths for Selected Elements and Compounds," Surf. Inter. Anal. 29, 108-114.
14. Gries, W.H., 1996, "A Universal Predictive Equation for the Inelastic Mean Free Pathlengths of X-ray Photoelectrons and Auger Electrons," Surf. Inter. Anal. 24, 38.
15. Zangwill, A., 1988, *Physics at Surfaces*, Cambridge Univ. Press, New York.
16. Somorjai, G.A., 1981, *Chemistry in Two Dimensions: Surfaces*, Cornell Press, Ithica.
17. Penn, D.R., 1976, "Electron Mean Free Paths for Free-electron-like Materials," Phys. Rev B, 13 5248.
18. Roth, J.A., R. Hoffmann, and J.R. Dennison, 2009, "Effects of Radiation Induced Conductivity on Electrostatic Discharge in Insulating Materials," in Proc. 1st AIAA Atmospheric and Space Environments Conf. (San Antonio, TX).
19. Dennison, J.R., J. Gillespie, J.L. Hodges, R.C. Hoffmann, J. Abbott, A.W. Hunt and R. Spalding, "Radiation Induced Conductivity of Highly-Insulating Spacecraft Materials," in *Application of Accelerators in Research and Industry*, Am. Instit. Phys. Conf. Proc. Series, Vol. 1099, ed. F.D. McDaniel and B. L. Doyle, (Am. Instit. of Phys., Melville, NY, 2009), pp. 203-208.
20. Yasuda, M., T. Nobuo and H. Kawata, 2004, "A Monte Carlo Calculation of Secondary Electron Emission from Organic Compounds," Jap. J. Appl. Phys., 43, 4004-4008.
21. Ashley, J. C. and M. W. Williams, 1980, "Electron Mean Free Paths in Solid Organic Insulators," Radiat. Res. 81, 364.
22. Burke E. A., 1980, "Secondary Emission from Polymers," IEEE Trans. NS, 27, 1760.



Greg Wilson received dual B.S. degrees in physics and mathematics from Utah State University in Logan, UT, where he is currently a graduate student in physics. He has worked with the Materials Physics Group for two years on electron emission and luminescence studies related to spacecraft charging.



J. R. Dennison received the B.S. degree in physics from Appalachian State University, Boone, NC, in 1980, and the M.S. and Ph.D. degrees in physics from Virginia Polytechnic Institute and State University (Virginia Tech), Blacksburg, in 1983 and 1985, respectively. He was a Research Associate with the University of Missouri—Columbia before moving to Utah State University (USU), Logan, in 1988. He is currently a Professor of physics at USU, where he leads the Materials Physics Group. He has worked in the area of electron scattering for his entire career and has focused on the electron emission and resistivity of materials related to spacecraft charging for the last two decades.